Evolution of Structural, Dielectric and Magnetic Properties of Cobalt Ferrite Nanoparticles Produced by Sol-Gel Technique During Sintering Treatment

Rihab Jabbar[1,*], Mohammed Hayder Ismail Alluaibi[2,*], Sara H. Shahatha[3] and Dhuha Sabah Hasan[4]

[1] Middle Technical University, Polytechnic College of Engineering - Baghdad, Baghdad, Iraq
[2] College of Energy and Environmental Sciences, Al-Karkh University of Science, 10081 Baghdad, Iraq
[3] Middle Technical University, Technical Engineering College, Baghdad, Iraq
[4] National Center of Hematology, Mustansiriyah University, Baghdad, Iraq

[*]Corresponding author: mohammed.alluaibi@kus.edu.iq

Abstract

This study investigates the effect of sintering temperature on the structural, dielectric and magnetic properties of cobalt ferrite nanoparticles ($CoFe_2O_4$ NPs) synthesized by the sol–gel method. The samples were sintered at 400°C–1000°C for 2 h and characterized using XRD, FTIR, SEM, AFM, dielectric and VSM measurements. XRD confirmed the formation of a stable cubic spinel structure, with crystallite size increasing from 10.71 to 16.09 nm and porosity decreasing with increasing sintering temperature. SEM and AFM showed progressive grain growth and improved grain connectivity, with the sample at 800°C exhibiting the most uniform morphology before excessive grain growth occurred at 1000°C. The dielectric response showed decreasing real and imaginary permittivity with increasing frequency, while the sample at 800°C exhibited the lowest dielectric loss (tan $\delta \approx 2$ at 1 kHz). Magnetic measurements revealed ferrimagnetic behavior, with saturation magnetization increasing from 27.5 emu/g at 400°C to 68 emu/g at 1000°C, whereas coercivity reached a maximum of 715 Oe at 800°C. Overall, sintering at 800°C provided the best balance between microstructural uniformity, low dielectric loss and magnetic performance, making it a strong candidate for further evaluation in high-frequency and multifunctional magnetic applications.

Keywords: Cobalt ferrite nanoparticles, sol-gel technique, sintering temperature, structural properties, dielectric properties, magnetic properties.

1. Introduction

Cobalt ferrite ($CoFe_2O_4$) is an inverse spinel ferrite that has attracted considerable interest because of its high chemical and thermal stability, moderate magnetocrystalline anisotropy, high coercivity, and useful electrical and magnetic properties [1–5]. These characteristics make $CoFe_2O_4$ nanoparticles ($CoFe_2O_4$ NPs) suitable for a wide range of applications, including magnetic and electromagnetic sensors, high-frequency electronic devices, electromagnetic interference (EMI) suppression, magnetic hyperthermia, drug delivery and other biomedical applications [3–5]. The functional properties of $CoFe_2O_4$ NPs are strongly influenced by their crystal structure, particle size, morphology, porosity, cation distribution and synthesis conditions.

Several techniques have been employed to synthesize $CoFe_2O_4$ NPs, including co-precipitation, hydrothermal processing, solid-state reactions and sol–gel methods [6–9]. Among these approaches, the sol–gel method provides good control over chemical composition and particle characteristics while enabling the preparation of relatively homogeneous and high-purity nanopowders at comparatively low processing temperatures [10–13]. In addition, it is relatively simple, cost-effective and suitable for producing nanostructured ferrites for magnetic, dielectric

[DOI: 10.22068/ijmse.4451]

and high-frequency applications [14–23]. These advantages make the sol–gel route appropriate for investigating the influence of subsequent thermal treatment on the functional properties of $CoFe_2O_4$ NPs.

The influence of heat treatment on the structural, dielectric and magnetic properties of cobalt ferrite has been investigated in several previous studies. Badr et al. [24] reported that annealing Ce-substituted cobalt ferrite between 600 and 1000°C increased both saturation and remanent magnetization, together with changes in grain size. Rahardjo et al. [6] observed an increase in crystallite size in Y-substituted cobalt ferrite with increasing treatment temperature, although the saturation magnetization decreased. Zhang et al. [25] found that increasing the sintering temperature of $CoFe_2O_4$ from 900 to 1300°C promoted grain growth and increased saturation magnetization, while coercivity decreased at higher temperatures. Silva et al. [26] also demonstrated a strong effect of heat-treatment temperature on the phase composition, morphology, and functional performance of sol–gel-derived $CoFe_2O_4$. Collectively, these studies confirm that thermal treatment is a key parameter controlling the microstructure and functional properties of $CoFe_2O_4$.

Although the general effects of sintering temperature on cobalt ferrite are well established, direct comparison of structural, dielectric and magnetic responses over a broad and identical set of processing conditions remains useful for identifying suitable conditions for multifunctional applications. Accordingly, the present study systematically evaluates sol–gel-prepared $CoFe_2O_4$ NPs sintered at 400°C, 600°C, 800°C and 1000°C for the same treatment duration. Structural and morphological evolution is correlated with dielectric and magnetic behavior using XRD, FTIR, SEM, AFM, dielectric measurements and vibrating sample magnetometry. Particular attention is given to identifying the sintering condition that achieves the best balance between crystallinity, microstructure, dielectric loss and magnetic performance rather than maximizing a single property. Therefore, this work is positioned as a systematic optimization study that extends previously reported trends and provides a comparative basis for selecting $CoFe_2O_4$ processing conditions for multifunctional and high-frequency applications.

2. Experimental Procedures

2.1. Synthesis of $CoFe_2O_4$ NPs

To produce cobalt ferrite nanoparticles ($CoFe_2O_4$ NPs), the sol-gel technique was used as a convenient procedure due to its precise control over the crystal structure and chemical composition. Initially, stoichiometric ratios of 0.5M cobalt chloride ($CoCl_2 \cdot 6H_2O$) and 1M ferric chloride ($FeCl_3$), both 98% pure and from BDH, were dissolved in distilled water (D.W.), with a ferric-to-cobalt molar ratio of 2:1. After initial solution preparation, 2M sodium hydroxide (NaOH) solution from Fluka (98% purity) was gradually added to the mixture in droplets, under continuous stirring for 90 minutes (see Table 1). The pH of the mixture was adjusted to 13 to ensure the appropriate basic conditions for gel formation. The initial heating was carried out at a constant temperature of 100 ±2°C, with continuous stirring for several hours until a dark and wet gel was formed. The gel

[DOI: 10.22068/ijmse.4451]

was then dried and ground into a fine powder. The resulting powder was washed several times with distilled water and alcohol to remove impurities such as sodium chloride produced during the reaction. After purification, the powder was subjected to a sintering treatment process in a German Nabertherm furnace. The samples were sintered at different temperatures (400°C, 600°C, 800°C and 1000°C) for 2 hours. This wide temperature range was designed to determine the optimal sintering conditions that achieve a functional balance between structural, dielectric and magnetic properties of $CoFe_2O_4$ NPs in multifunctional applications. Fig. 1 shows the complete sequence of preparation steps using the sol-gel technique, from the preparation of chemical solutions to the sintering process of $CoFe_2O_4$ NPs.

Table 1. Chemicals used in the synthesis of $CoFe_2O_4$ NPs.

Chemicals	Formula	Purity (%)	Company	Weights (g)	D.W. (ml)
Ferric chloride	$FeCl_3$	98	BDH	8.19	50
Cobalt chloride	$CoCl_2.6H_2O$	98	BDH	6	50
Sodium hydroxide	NaOH	98	Fluka	8	100

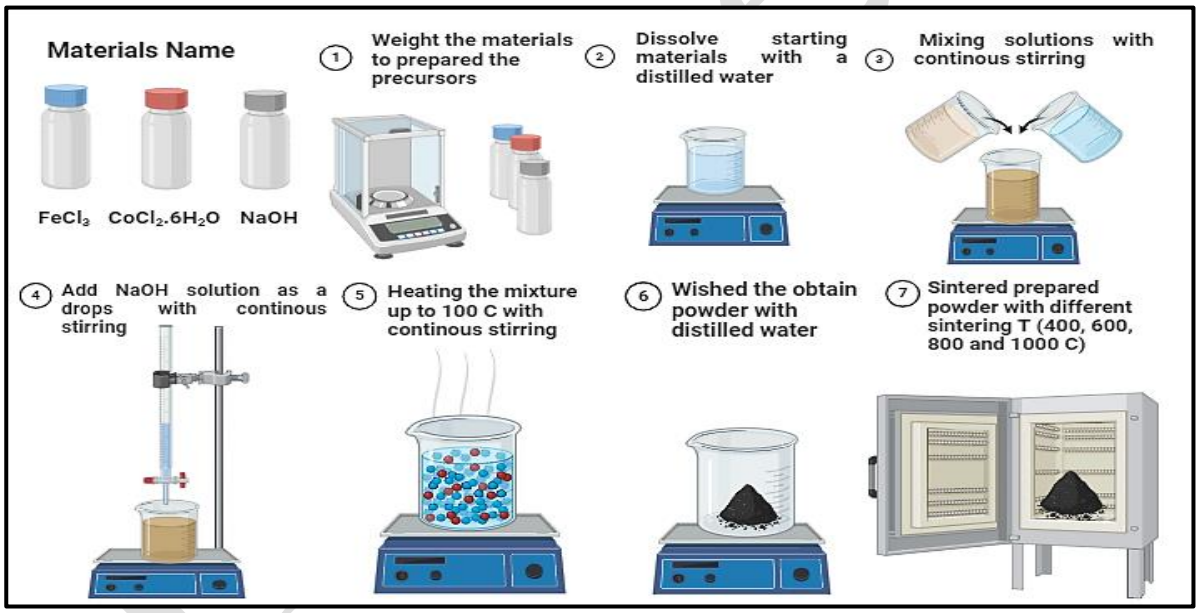

Fig. 1. Preparation steps of $CoFe_2O_4$ NPs at different sintering temperatures.

2.2. Characterization

Structural, morphological, dielectric and magnetic characterization was performed using X-ray diffraction (XRD) - (ADX-2500, Cu-Kα, λ = 1.54060 Å), scanning electron microscopy (SEM) - (FEI Inspect S50), atomic force microscopy (AFM) - (Angstrom Advanced Inc.), Fourier transform infrared (FTIR) spectroscopy (SHIMADZU-8400S; 400–4000 cm^{-1}), an LCR meter (MICROTEST) and vibrating-sample magnetometer (VSM) measurements at room temperature under an applied field of ±15 kOe.

[DOI: 10.22068/ijmse.4451]

3. Results and Discussion

3.1. Structural and morphological analysis

The structural parameters of $CoFe_2O_4$ NPs were derived from the XRD data using standard relations. The crystallite size (D), lattice constant (a), X-ray density (ρx), estimated specific surface area (S), porosity (P) and hopping lengths at tetrahedral (L_A) and octahedral (L_B) sites were calculated as follows using Eqs. (1) – (6) [28–31]:

$$D = \frac{0.9\,\lambda}{\beta \cos\theta} \tag{1}$$

$$a = d_{hkl}\sqrt{h^2 + k^2 + l^2} \tag{2}$$

$$\rho_x = \frac{8M}{N_A\, a^3} \tag{3}$$

Where: M - molecular weight of $CoFe_2O_4$ NPs; N - Avogadro number and a - lattice constant.

$$S = \frac{6000}{D\,\rho_X} \tag{4}$$

$$P\,(\%) = \left(1 - \frac{\rho_m}{\rho_X}\right) \times 100 \tag{5}$$

Where: P - porosity percentage; ρ_m - mass density and ρ_x - X-ray density.

$$L_A = 0.4325\ (a);\ L_B = 0.3525\ (a) \tag{6}$$

The XRD patterns in Fig. 2 confirm the formation of a single-phase cubic spinel $CoFe_2O_4$ structure with $Fd\bar{3}m$ symmetry, which corresponds well to JCPDS card No. 22-1086. The characteristic reflections corresponding to the (220), (311), (222), (400), (422), (511) and (440) planes were observed, with no detectable secondary phases. At higher sintering temperatures, particularly above 600°C, the (311) reflection showed a slight shift toward lower 2θ, accompanied by sharper diffraction peaks, indicating changes in lattice strain and improved crystallinity. As shown in Fig. 3a and Table 2, the crystallite size increased from 10.71 to 16.09 nm with increasing sintering temperature, reflecting thermally activated crystallite growth and coalescence. These values are comparable with those previously reported for $CoFe_2O_4$ prepared by related synthesis routes (Table 3) [32–36]. The lattice constant remained nearly unchanged between 400°C and 600°C and then subsequently increased, reaching 8.3753 Å at 1000°C, which may be associated with heat-induced lattice expansion and/or localized structural strain redistribution [37]. The hopping lengths L_A and L_B showed a similar variation because both depend directly on the lattice constant.

[DOI: 10.22068/ijmse.4451]

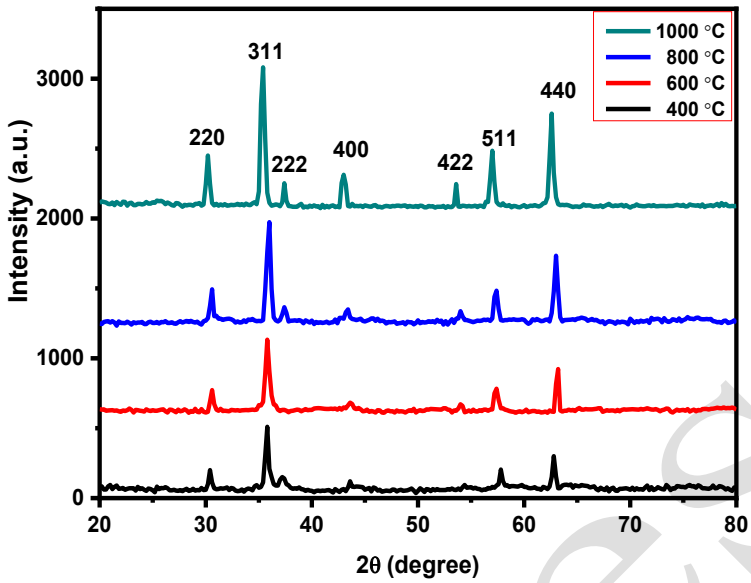

Fig. 2. XRD patterns of $CoFe_2O_4$ NPs at different sintering temperatures.

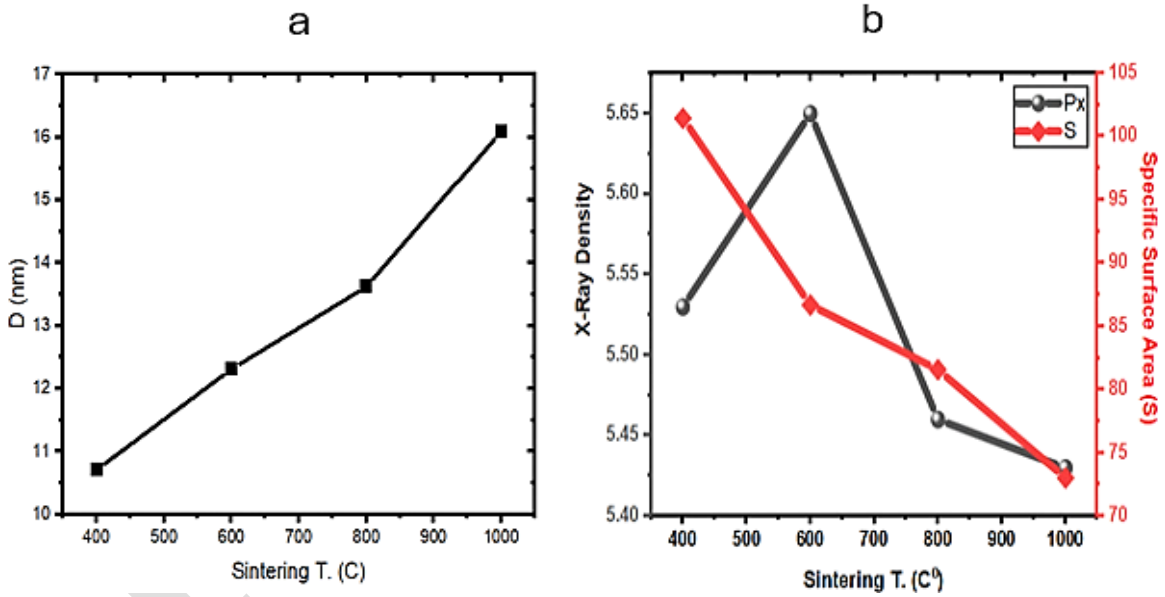

Fig. 3. Variation of crystallite size (a) and X-ray density and specific surface area as a function of sintering temperature (b).

The dislocation density (δ) and microstrain (ε) of the $CoFe_2O_4$ NP samples were calculated using Eqs. (7) and (8) [38]:

$$\delta = \frac{1}{D^2} \tag{7}$$

$$\varepsilon = \frac{\beta \cos\theta}{4} \tag{8}$$

[DOI: 10.22068/ijmse.4451]

Similar XRD-based analyses of structural evolution in nanostructured ferrite and oxide systems have also been reported [39, 40]. With increasing sintering temperature, crystallite size increased while both microstrain and dislocation density decreased, indicating improved crystallinity and reduced structural defects. The specific surface area also decreased, along with a drop in porosity from 65% to 34%, which is consistent with progressive densification. The X-ray density showed only a slight non-monotonic variation, as shown in Table 2.

Table 2. XRD parameters of $CoFe_2O_4$ NPs at different sintering temperatures.

Sintering Temperatures (°C)	**D (nm)**	**a (A°)**	**d_{311} (A°)**	**ρ_x (g/cm³)**	**S (m^2/g)**	**P (%)**	**L_A**	**L_B**	**Dislocation density (δ) x 10^{15} (m^{-2})**	**ϵ**	**Volume of unit cell $a = b =$ c (Å³)**
400	10.71	8.1874	2.4686	5.679	101.5	65	3.545	2.895	8.7181	0.167	548.83
600	12.31	8.1838	2.4675	5.686	86.8	62	3.544	2.893	6.5991	0.122	548.11
800	13.62	8.2986	2.5021	5.454	81.9	49	3.593	2.934	5.3907	0.111	571.50
1000	16.09	8.3753	2.5252	5.305	73.2	34	3.627	2.961	3.8627	0.082	587.49

Table 3. Comparison of XRD parameters of $CoFe_2O_4$ NPs with other works.

Synthesis method	**Heat treatment temperature (°C)**	**D (nm)**	**a (A°)**	**Ref.**
PEG-assisted sol-gel method	300 – 800	7.6 – 12.8	~ 8.39	[32]
Co-precipitation method	600 – 750	15.96 – 19.11	8.2940 – 8.3313	[34]
Green synthesis of the sol-gel method	200 – 750	3.7 – 9.4	8.0688 – 8.3779	[37]
Hydrothermal method	As prepared, 700 – 800	43.49 – 53.85	8.391 – 8.400	[41]
Sol-gel auto-combustion method	200 – 1000	26.38 – 56.53	8.3801 – 8.3937	[42]
Sol-gel precipitation method	400 – 1000	10.71 – 16.09	8.1838 – 8.3753	Present work

Fig. 4 shows SEM images that reveal the gradual evolution of the microstructure with increasing sintering temperature. At 400°C (Fig. 4a), the grains are relatively small (28 ± 4 nm), irregularly distributed and separated by visible voids, indicating incomplete densification. At 600°C (Fig. 4b), partial coalescence occurs and the average grain size increases to 39 ± 6 nm. At 800°C (Fig. 4c), larger and more interconnected grains (53 ± 5 nm) are observed, indicating advanced sintering and improved grain connectivity. Further heating to 1000°C (Fig. 4d) produces pronounced coalescence and excessive grain growth, with an average grain size of 65 ± 5 nm. Overall, increasing temperature promotes diffusion and grain-boundary migration, leading to grain growth and reduced porosity, in agreement with the XRD results. Fig. 5 shows 3D AFM surface morphology of $CoFe_2O_4$ NPs at different sintering temperatures. The surface becomes

[DOI: 10.22068/ijmse.4451]

progressively more homogeneous from 400°C to 800°C (Figs. 5a to 5c), indicating improved recrystallization and grain connectivity. The sample at 800°C exhibits the most uniform surface morphology, whereas further heating to 1000°C (Fig. 5d) leads to marked grain growth and increased surface roughness due to particle coalescence. These observations are consistent with the SEM and XRD results.

FTIR spectroscopy was used to confirm the characteristic metal–oxygen vibrations of the spinel $CoFe_2O_4$ structure and to assess the effect of sintering temperature on the local bonding environment. As shown in Fig. 6, the higher-wavenumber bands at 516.94–592.17 cm^{-1} are attributed to M–O vibrations at the tetrahedral A-site, whereas the lower-wavenumber bands at 408.92–499.58 cm^{-1} correspond to M–O vibrations at the octahedral B-site. The presence of these bands in all samples confirms the preservation of the spinel structure throughout the investigated temperature range. Their shifts and splitting with increasing sintering temperature indicate changes in the local M–O environment, which are likely associated with lattice distortion, defect evolution and possible cation redistribution. However, FTIR band splitting alone is insufficient to quantitatively determine the degree of cation inversion. Additional bands at higher wavenumbers are attributed mainly to surface hydroxyl groups, adsorbed moisture and carbon-containing residual species. The main vibrational assignments are summarized in Table 4.

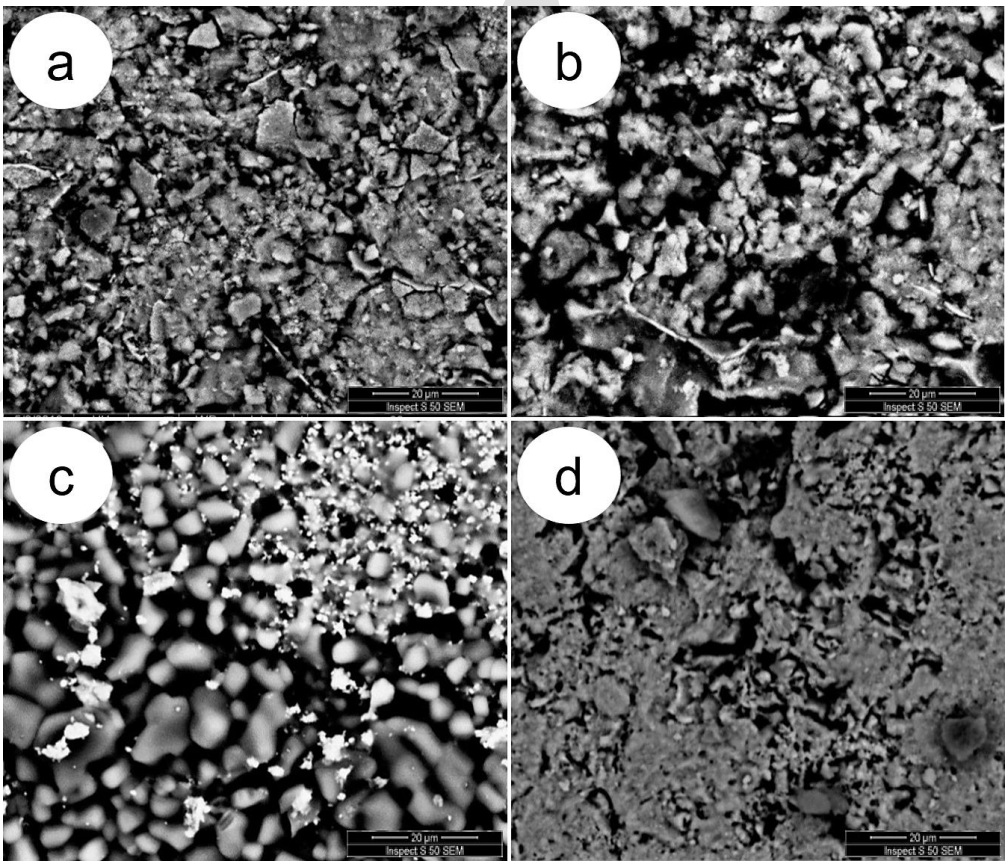

Fig. 4. SEM images of $CoFe_2O_4$ NPs at different sintering temperatures: 400°C (a), 600°C (b), 800°C (c) and 1000°C (d).

[DOI: 10.22068/ijmse.4451]

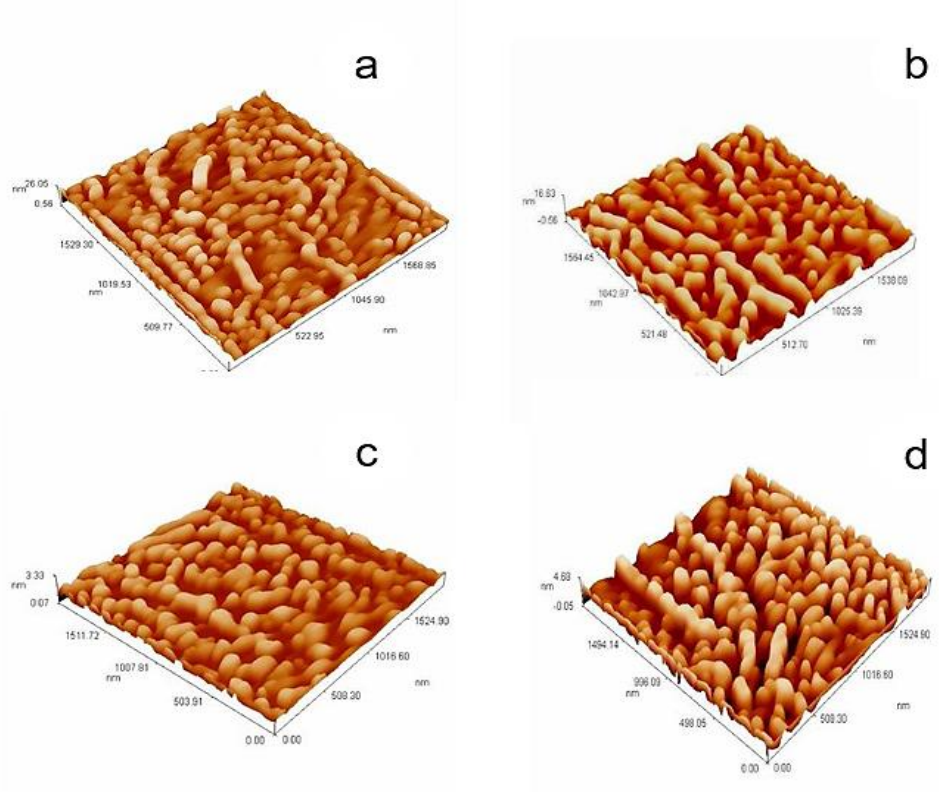

Fig. 5. 3D AFM images of $CoFe_2O_4$ NPs at different sintering temperatures: 400°C (a), 600°C (b), 800°C (c) and 1000°C (d).

To further evaluate the effect of sintering temperature on the local metal–oxygen bonding, the force constants associated with the tetrahedral and octahedral sites were calculated from the corresponding FTIR wavenumbers using [43]:

$$F = 4\pi^2 c^2 \mu\nu^2 \quad (9)$$

Where: F - force constant; c - speed of light; μ - reduced mass of the vibrating metal–oxygen pair and ν - corresponding FTIR wavenumber. The average force constant (F_{av}), when both tetrahedral (F_T) and octahedral (F_o) contributions are available as a corresponding pair, was estimated from [43]:

$$F_{av} = \frac{F_T + F_o}{2} \quad (10)$$

[DOI: 10.22068/ijmse.4451]

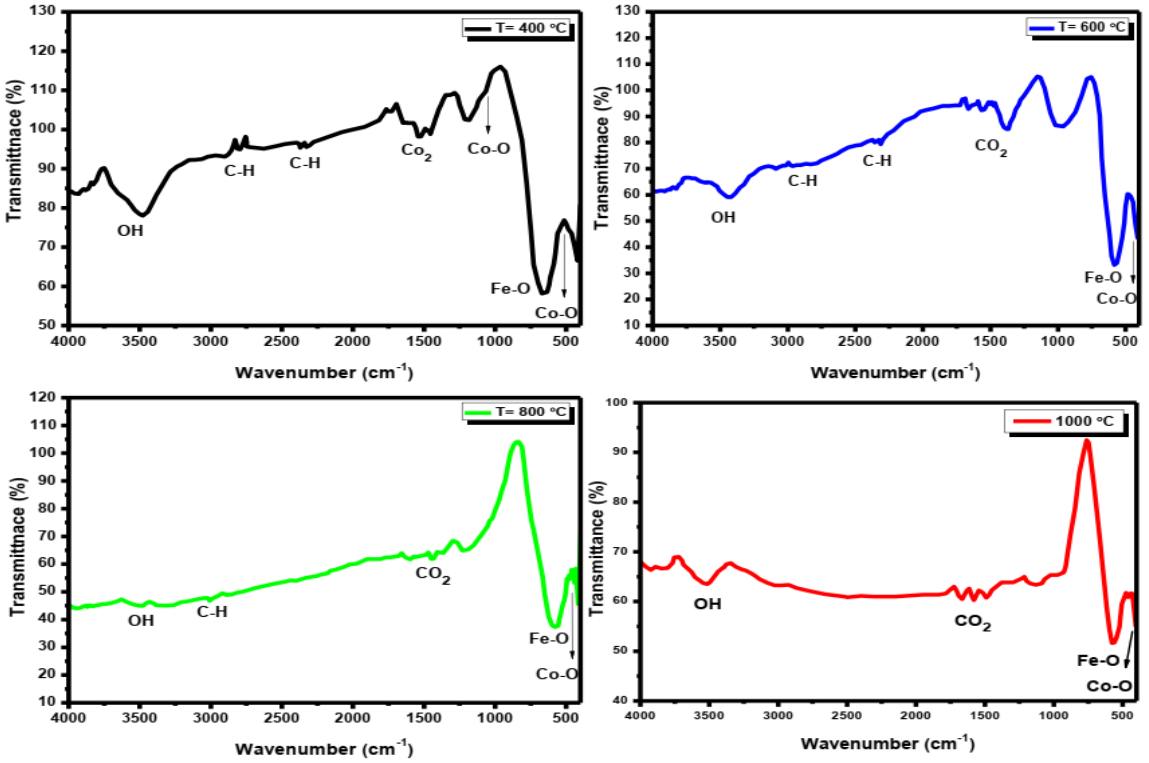

Fig. 6. FTIR pattern of $CoFe_2O_4$ NPs at different sintering temperatures.

Table 4. Functional groups identified in $CoFe_2O_4$ NPs synthesized at different sintering temperatures.

Sintering temperatures	M_{octa}–O	M_{tetra}–O	Co-sub. spinel ferrites Group	Sym. & assym. stretching vibration of CO_2	Aliphatic & aromatic C–H bond	C-H stretching bands	OH-group
400°C	499.58	592.17	1065.03	1561.10 1560.45 1632.89 1700.34	2226.58 2362.88 2362.88	2744.49 2878.01 3030.30	3305.33 3459.81
600°C	416.64 457.14	572.88	—	1440.90 1470.74 1580.29 1650.13	2330.44 2588.31	2785.30 3005.20	3443.76
800°C	443.64 484.15	585.52 592.17	1077.53	1470.16 1519.51 1527.34 1688.88	3103.14	—	3430.70 3476.65
1000°C	408.92	516.94 574.81 588.31	1078.24	1536.12 1578.13 1601.28 1633.51	2362.88	3130.27	3448.84

[DOI: 10.22068/ijmse.4451]

Similar FTIR-based evaluations of tetrahedral and octahedral force constants and their average have also been reported for related spinel ferrite systems [44–46]. The force constants associated with the tetrahedral and octahedral sites were calculated separately for each resolved M–O vibrational component using Eq. (9). The higher-wavenumber components (ν_1) were assigned to tetrahedral A-site vibrations and were therefore used to calculate F_T, whereas the lower-wavenumber components (ν_2) were assigned to octahedral B-site vibrations and were used to calculate F_O. Accordingly, multiple F_T or F_O values at a given sintering temperature arise from resolved/split vibrational components within the same sample and do not represent different samples. The average force constant (F_{av}) was calculated only when a corresponding tetrahedral–octahedral vibrational pair was available; otherwise, it was not determined. The resulting force constants are summarized in Table 5.

Table 5. Vibrational properties of $CoFe_2O_4$ NPs at different sintering temperatures.

Sintering temperatures (°C)	$\upsilon_{1\ cm^{-1}}$	$\upsilon_{2\ cm^{-1}}$	$F_T \times 10^5$ (dyne/cm)	$F_o \times 10^5$ (dyne/cm)	$F_{av} \times 10^5$ (dyne/cm)	**Ref.**
400	592.17	499.58	2.57	1.83	2.19	Present work
600	572.88	416.64	2.41	1.27	1.83	
	—	457.14	—	1.53	—	
800	585.52	443.64	2.51	1.44	1.97	
	592.17	484.15	2.57	1.72	2.14	
1000	516.94	408.92	1.96	1.23	1.59	
	574.81	—	2.42	—	—	
	588.31	—	2.54	—	—	
400	584.46	382.89	2.53	1.07	1.80	[6]
800	599.67	355.24	2.63	0.92	1.77	[45]
500	570	364	2.37	0.96	1.67	[47]

3.2. Dielectric properties

The dielectric properties of spinel ferrites, such as $CoFe_2O_4$ NPs, are generally appropriate for use in high-frequency devices, and new possible uses are continuously being investigated. The synthesis process, material composition, sintering temperature and time are important factors in regulating the characteristics of these dielectric materials [41].

The dielectric loss factor (tan δ), the real part of the dielectric constant (ε') and the imaginary part of the dielectric constant (ε") were determined using the following equations [46]:

$$\varepsilon' = \frac{C\,d}{\varepsilon_o\,A} \tag{11}$$

$$\varepsilon'' = \varepsilon' \tan\delta \tag{12}$$

Fig. 7 shows the frequency-dependent dielectric properties at room temperature of $CoFe_2O_4$ NPs sintered at different temperatures. Both ε′ and ε″ decrease with increasing frequency over the

[DOI: 10.22068/ijmse.4451]

investigated sintering-temperature range (Figs. 7a and 7b). This dispersion is consistent with the Maxwell–Wagner interfacial polarization mechanism and Koops' model, in which charge accumulation at resistive grain boundaries enhances polarization at low frequencies, whereas charge carriers are unable to follow the rapidly varying electric field at high frequencies [47–50]. Fig. 7c shows the frequency dependence of the dielectric loss factor (tan δ) at different sintering temperatures. At 1 kHz, tan δ decreases from 4.03 at 400°C to a minimum value of approximately 2 at 800°C, before increasing to 3.1 at 1000°C. The sample sintered at 800°C exhibited the lowest dielectric loss at 1 kHz among the investigated samples. The dielectric response of $CoFe_2O_4$ is mainly associated with electron hopping between Fe^{+2}/Fe^{+3} ions and hole hopping involving Co^{+2}/Co^{+3} ions [41]. As shown in Fig. 7d, both ε′ and ε″ at 1 kHz decrease with increasing sintering temperature, which can be attributed to grain growth and the consequent reduction in grain-boundary and interfacial polarization contributions [51]. Table 6 shows the dielectric properties of $CoFe_2O_4$ NPs, including the real part of the dielectric constant (ε′), the imaginary part (ε″) and the dielectric loss factor (tan δ), which were measured at different frequencies and sintering temperatures. The observed values are consistent with the frequency- and temperature-dependent dielectric behavior discussed above.

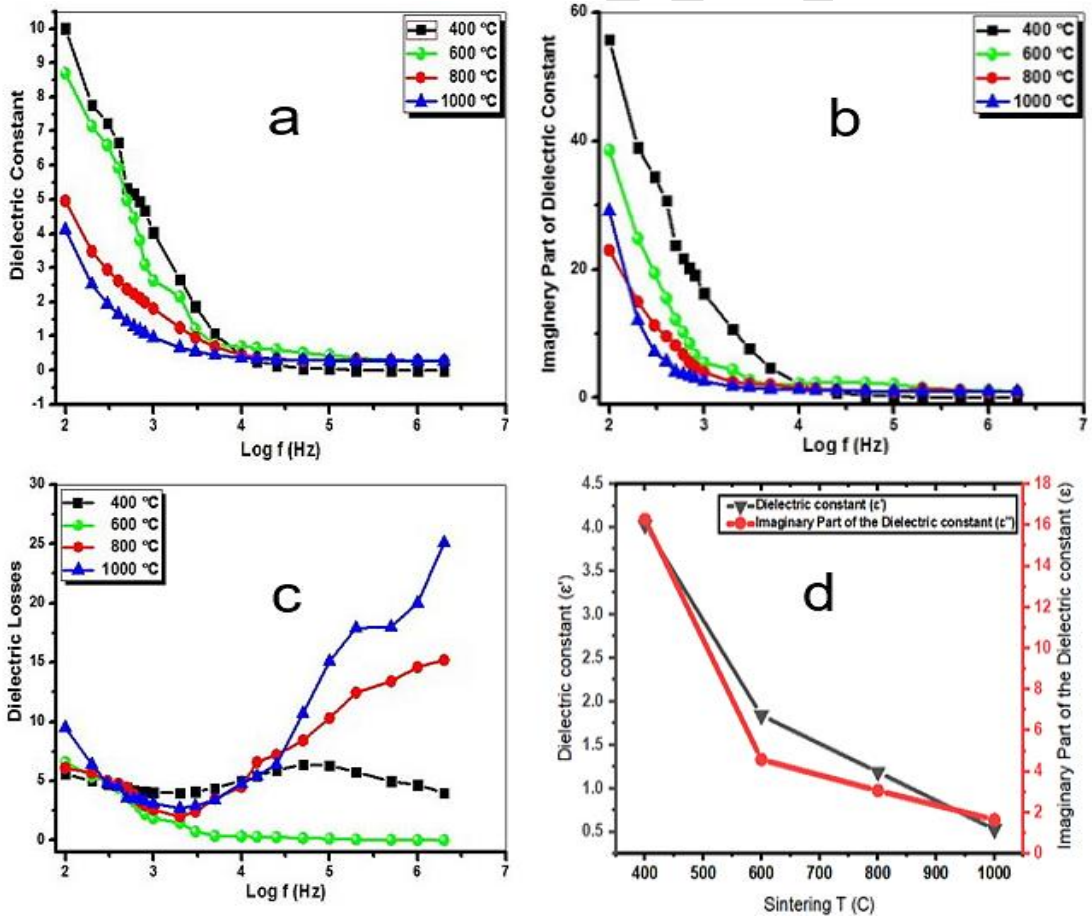

Fig. 7. Schematic representations of variation of dielectric constant (a), imaginary part of dielectric constant (b), dielectric losses factor with frequency (c) and value of dielectric constant and imaginary part of dielectric constant as a function of sintering temperatures at 1 kHz (d).

[DOI: 10.22068/ijmse.4451]

Table 6. Dielectric properties of $CoFe_2O_4$ NPs at different frequencies as a function of sintering temperatures.

Sintering temperature (°C)	Dielectric constant (ε')			Imaginary part of dielectric constant (ε'')			Dielectric losses factor (tan δ)		
	100 Hz	1 kHz	1 MHz	100 Hz	1 kHz	1 MHz	100 Hz	1 kHz	1 MHz
400	10.01	4.03	10^{-3}	55.76	16.27	$4x10^{-3}$	5.57	4.03	4.67
600	6.58	1.84	0.01	38.21	4.58	0.21	5.8	2.38	11.6
800	3.66	1.19	$6x10^{-4}$	22.37	3.07	$5x10^{-3}$	6.1	2	15.2
1000	3	0.53	$9x10^{-4}$	28.55	1.65	0.02	9.5	3.1	25.1

The AC conductivity (σ) was calculated using the following relationships (13 and 14) [41]:

$$\sigma = \varepsilon' \varepsilon_0 \omega \tan \delta \quad (13)$$

Where: ω - angular frequency

$$\omega = 2\pi f \quad (14)$$

Where: f - frequency.

Fig. 8 shows the frequency-dependent AC conductivity (σ) of $CoFe_2O_4$ NPs sintered at 400–1000°C at room temperature. In general, AC conductivity increases with frequency, consistent with the Maxwell–Wagner model and electron hopping between Fe^{+2}/Fe^{+3} ions at octahedral B-sites. At low frequencies, charge accumulation at resistive grain boundaries limits conduction, whereas at higher frequencies, enhanced charge-carrier hopping within the grains leads to increased AC conductivity [52]. Regarding the effect of sintering temperature, the sample at 600°C exhibited the highest conductivity, whereas the samples at 800°C and 1000°C maintained comparatively lower values over the measured frequency range. The sample at 400°C showed a distinct non-monotonic response, with conductivity reaching a maximum near 1 kHz, followed by a decrease, and then a slight recovery at higher frequencies. Its small crystallite size (≈10.71 nm), high defect density and larger contribution of resistive grain boundaries may influence this response. However, these factors alone cannot fully explain the observed maximum value. The relaxation-related processes or electrode/contact effects may also contribute. Therefore, without additional impedance or electrode-control measurements, the exact origin of this feature cannot be conclusively determined and requires further investigation [53].

[DOI: 10.22068/ijmse.4451]

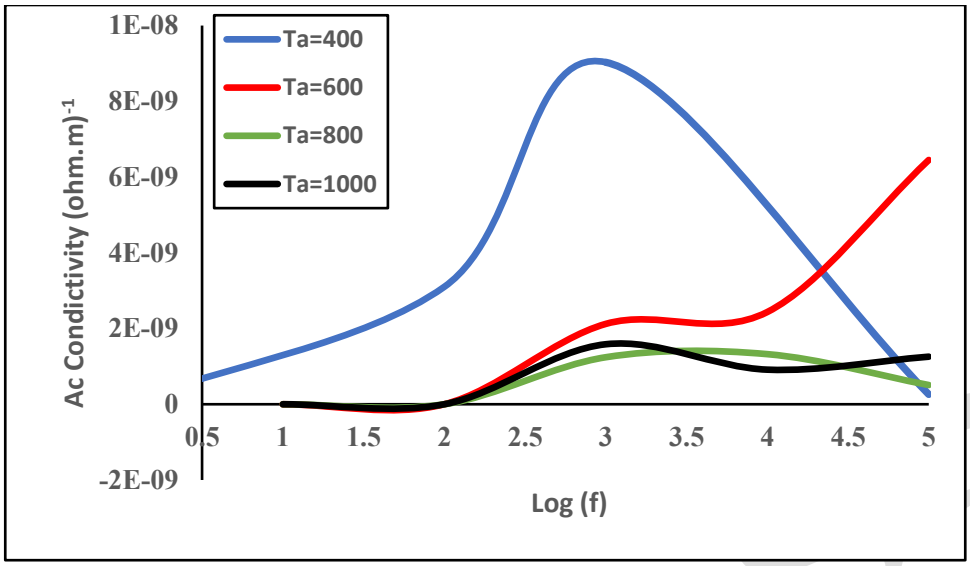

Fig. 8. AC conductivity of $CoFe_2O_4$ NPs at different frequencies as a function of sintering temperatures.

3.3. Magnetic properties

Fig. 9 shows the room-temperature M–H hysteresis loops of $CoFe_2O_4$ NPs sintered at 400, 600, 800 and 1000°C. All samples exhibit ferrimagnetic hysteresis behavior, with systematic changes in saturation magnetization (M_s), remanent magnetization (M_r) and coercivity (Hc) as a function of sintering temperature. The corresponding magnetic parameters calculated from the hysteresis loops are summarized in Table 7. The magnetic moment per formula unit can be found using hysteresis loops at room temperature from the following equation [28]:

$$\mu B = \frac{M \times M_S}{5585} \tag{15}$$

The saturation and remanent magnetizations increased with sintering temperature, as shown in Fig. 10a, with M_s increasing from 27.5 emu/g at 400°C to 68 emu/g at 1000°C. This behavior is mainly attributed to grain growth, improved crystallinity, stronger exchange interactions and reduced surface-spin disorder, in agreement with previous studies [6, 27, 48, 54, 55]. However, the M_s values remained below the bulk value of $CoFe_2O_4$ (80.8 emu/g), which can be explained by finite-size effects and spin disorder at the nanoparticle surface [48, 49]. The maximum Ms value obtained in the present study is also comparable to values reported for $CoFe_2O_4$ NPs in previous studies [56, 57]. Table 7 shows relatively low remanence ratios (M_r/M_s = 0.17–0.36). According to the Stoner–Wohlfarth model, these values are lower than the expected ideal value for non-interacting single-domain particles with randomly oriented easy axes, indicating a large contribution from uniaxial anisotropy. The coercivity increased from 209 Oe at 400°C to a maximum of 715 Oe at 800°C, and then decreased to 211 Oe at 1000°C, as shown in Fig. 10b. The initial increase is associated with enhanced magnetic anisotropy and grain growth, whereas the subsequent decrease at 1000°C is attributed to the transition toward a multidomain structure and easier domain-wall motion [58]. Thus, the sample at 800°C exhibits the highest resistance to magnetization reversal. The magnetic

[DOI: 10.22068/ijmse.4451]

moment of ideal inverse-spinel $CoFe_2O_4$ is 3.0 μB per formula unit at 0 K, according to the collinear Néel model. In the present samples, μB increased from 1.15 to 2.88 μB with increasing sintering temperature. The lower experimental μB values may be associated with surface spin disorder, spin canting, finite-size effects, structural defects and possible changes in cation distribution [59]. Therefore, the increase in μB with sintering temperature is mainly attributed to improved magnetic ordering and reduced surface-spin disorder. However, the degree of cation inversion cannot be quantitatively determined from the present room-temperature magnetic measurements alone. Among the investigated samples, the sample at 800°C showed the best overall balance between microstructural uniformity, low dielectric loss and magnetic performance (M_s = 51 emu/g and Hc = 715 Oe), and was therefore selected as the optimum sintering condition for multifunctional applications. Table 8 compares the magnetic parameters obtained in the present work with values reported in recent studies. Considerable variations in M_s and Hc are observed in the literature, reflecting differences in synthesis routes, crystallite/grain sizes, cation distributions and heat-treatment conditions. The present sample at 800°C (M_s = 51 emu/g and Hc = 715 Oe) is within the reported range and shows a balanced magnetic response, whereas the sample at 1000°C shows a higher M_s but markedly lower Hc.

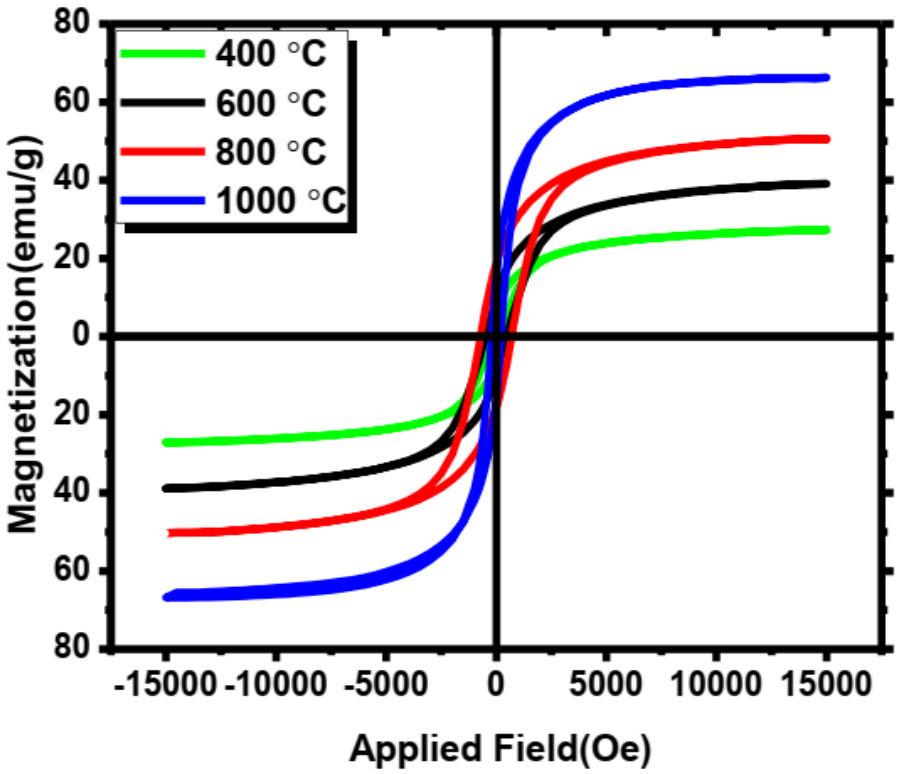

Fig. 9. VSM of $CoFe_2O_4$ NPs at different sintering temperatures.

[DOI: 10.22068/ijmse.4451]

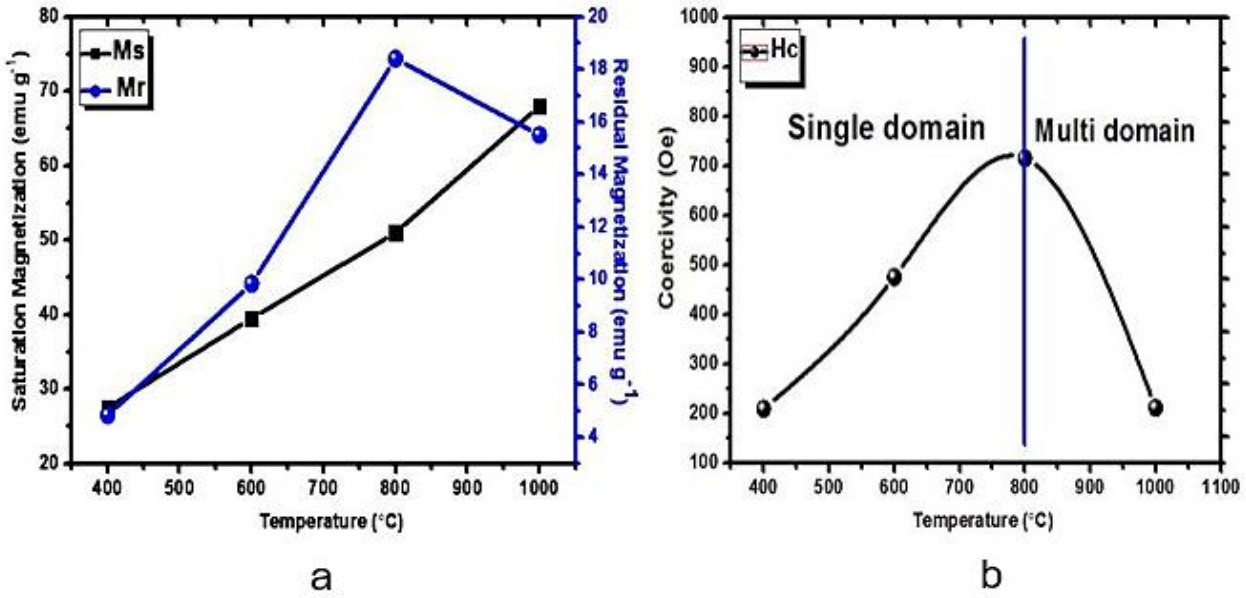

Fig. 10. Effect of sintering temperature on (a) saturation magnetization (M_s) and remanent magnetization (M_r) and (b) coercivity (Hc) of $CoFe_2O_4$ NPs.

Table 7. Magnetic parameters of $CoFe_2O_4$ NPs at different sintering temperatures.

Sintering Temperature (°C)	(M_s) (emu g^{-1})	(M_r) (emu g^{-1})	(Hc) (Oe)	(M_r/M_s) ratio	μB (B.M.)
400	27.5	4.84	209	0.17	1.15
600	39.5	9.84	475	0.24	1.66
800	51	18.4	715	0.36	2.14
1000	68	15.5	211	0.22	2.88

Table 8. Comparison of magnetic parameters of $CoFe_2O_4$ NPs with other works.

Ref.	Heat treatment temperature (°C)	D (nm)	M_s (emu g^{-1})	Hc (Oe)	M_r/M_s ratio	μB (B.M.)
[6]	400	16.05	30.79	1588	0.39	1.29
[25]	1300	830	87.32	1368.33	0.19	—
[32]	800	12.80	85.5	1920	0.36	—
[39]	600	56.27	73	1958	0.52	—
[41]	800	53.85	46.20	467.73	0.47	1.94
[42]	1000	56.53	77.94	679	0.27	3.27
[56]	600	13.98	68.03	1439.59	0.48	—
[60]	700	21	41	580	0.30	1.72
[61]	900	40	84.97	720	0.30	3.57
[62]	600	25.32	50	1100	0.42	—

[DOI: 10.22068/ijmse.4451]

[63]	800	55.60	72.58	1005.33	0.47	3.05
[64]	1200	—	80.03	189.1	0.12	—
[65]	500	24.11	50.60	1077	0.56	2.26
Present work	800	13.62	51	715	0.36	2.14
	1000	16.09	68	211	0.22	۲.88

4. Conclusions

$CoFe_2O_4$ NPs were successfully synthesized by the sol–gel method and sintered at 400, 600, 800 and 1000°C to evaluate the influence of sintering temperature on their structural, dielectric, and magnetic properties. XRD analysis confirmed the formation of a stable cubic spinel structure, while increasing the sintering temperature enhanced crystallinity and grain connectivity and reduced structural defects and porosity, accompanied by increases in crystallite and grain sizes. The dielectric response showed a general decrease in the real and imaginary parts of the permittivity with increasing frequency. In contrast, the sample sintered at 800°C exhibited the lowest dielectric loss ($\tan \delta \approx 2$ at 1 kHz). Magnetic measurements showed an increase in saturation magnetization with sintering temperature, reaching 68 emu/g at 1000°C, while coercivity reached its maximum value of 715 Oe at 800°C. Despite the higher saturation magnetization obtained at 1000°C, the associated excessive grain growth and deterioration in dielectric performance indicate a trade-off between magnetic and dielectric properties. Therefore, the sample sintered at 800°C provides the most favorable overall balance, with a crystallite size of 13.62 nm, Ms = 51 emu/g, Hc = 715 Oe and relatively low dielectric loss, making it a strong candidate for further evaluation in high-frequency and multifunctional magnetic applications. Future work should directly evaluate the electromagnetic interference shielding effectiveness of the 800°C sample in the X-band (8–12 GHz) and investigate the stability of its magnetic properties under repeated thermal cycling.

References

[1] Dojcinovic, M. P., Vasiljevic, Z. Z., Pavlovic, V. P., Barisic, D., Pajic, D., Tadic, N. B. and Nikolic, M. V., *"Mixed Mg–Co spinel ferrites: Structure, morphology, magnetic and photocatalytic properties," J. Alloys Compd.*, 2021, 855(1), 157429.

[2] Caldeira, L. E., *"Synthesis, Properties, and Applications of Spinel Cobalt Ferrites,"* in *Environmental Applications of Nanomaterials*, 1st ed., A. K. Alves, Ed., Springer Cham, Switzerland, 2022, 1-16.

[3] Abimathi, N., Harshene, H. and Vidhya, B., *"Synthesis and characterization of $CoFe_2O_4$ nanoparticles with its medical application," Mater. Today Proc.*, 2022, 62(4), 2315-2319.

[4] Ansari, M. A., Govindasamy, R., Begum, M. Y., Ghazwani, M., Alqahtani, A., Alomary, M. N., Jamous, Y. F., Alyahya, S. A., Asiri, S., Khan, F. A., Almessiere, M. A. and Baykal, A., *"Bioinspired ferromagnetic $CoFe_2O_4$ nanoparticles: Potential pharmaceutical and medical applications," Nanotechnol. Rev.*, 2023, 12(1), 20230575.

[5] García-Morales, N. A., García-Limón, V., Aguilar-Mejía, Ó. E., Reyes-Cruz, H. and Suaste-Gómez, E., *"Ferrimagnetic Ceramic of $CoFe_2O_4$ as a Temperature Sensor with Its Potential Application in the Biomedical Engineering Field,"* in *X Latin American Congress on Biomedical Engineering*, 1st ed., F. M. Martinez-Licona, V. L. Ballarin, E. A. Ibarra-Ramírez, S. M. Perez-Buitrago and L. R. Berriere, Eds., Springer Cham, Switzerland, 2025, 157-168.

[DOI: 10.22068/ijmse.4451]

[6] Rahardjo, D. T., Budiawanti, S., Suharno, S., Suryana, R., Supriyanto, A. and Purnama, B., *"Decreasing of Magnetic Saturation of Yttrium Doped Cobalt Ferrite Prepared by the Sol-Gel Auto-Combustion," Trends Sci.*, 2024, 21(4), 7320.

[7] Nasrin, S., Chowdhury, F. U. Z. and Hoque, S. M., *"Study of hyperthermia temperature of manganese-substituted cobalt nano ferrites prepared by chemical co-precipitation method for biomedical application," J. Magn. Magn. Mater.*, 2019, 479, 126-134.

[8] Fayazzadeh, S., Khodaei, M., Arani, M., Mahdavi, S. R., Nizamov, T. and Majouga, A., *"Magnetic Properties and Magnetic Hyperthermia of Cobalt Ferrite Nanoparticles Synthesized by Hydrothermal Method," J. Supercond. Nov. Magn.*, 2020, 33(7), 2227-2233.

[9] Islam, M. A., Hossain, A. K. M. A., Ahsan, M. Z., Bally, M. A. A., Ullah, M. S., Hoque, S. M. and Khan, F. A., *"Structural characteristics, cation distribution, and elastic properties of Cr^{3+} substituted stoichiometric and non-stoichiometric cobalt ferrites," RSC Adv.*, 2022, 12(14), 8502-8519.

[10] Aziz, C. and Azhdar, B., *"Synthesis of dysprosium doped cobalt ferrites nanoparticles by solgel auto-combustion method and influence of grinding techniques on structural, Morphological, and magnetic properties," J. Magn. Magn. Mater.*, 2022, 542, 168577.

[11] Solunke, A., Barote, V. K., Sonawane, B., Shirsath, S. E., Kadam, R. H. and Shinde, V. S., *"Sol-gel synthesis of Fe-rich cobalt ferrite nanoparticles and influence of pH concentration," Mater. Today Proc.*, 2023, 92(2), 1225-1230.

[12] Brinker, C. J. and Scherer, G. W., *Sol-Gel Science: The Physics and Chemistry of Sol-Gel Processing*, 1st ed., Academic Press, 2013, 924.

[13] Attia, S. M., Jue, W., Guangming, W. U., Jun, S. and Jianhua, M. A., *"Review on sol-gel derived coatings: Process, techniques and optical applications," J. Mater. Sci. Technol.*, 2002, 18(03), 211.

[14] Abid, N., Khan, A. M., Shujait, S., Chaudhary, K., Ikram, M., Imran, M., Haider, J., Khan, M., Khan, Q. and Maqbool, M., *"Synthesis of nanomaterials using various top-down and bottom-up approaches, influencing factors, advantages, and disadvantages: A review," Adv. Colloid Interface Sci.*, 2022, 300, 102597.

[15] Khan, Y., Sadia, H., Shah, S. Z. A., Khan, M. N., Shah, A. A., Ullah, N., Ullah, M. F., Bibi, H., Bafakeeh, O. T., Khedher, N. B., Eldin, S. M., Fadhl, B. M. and Khan, M. I., *"Classification, Synthetic, and Characterization Approaches to Nanoparticles, and Their Applications in Various Fields of Nanotechnology: A Review," Catalysts*, 2022, 12(11), 1386.

[16] Harish, V., Ansari, M. M., Tewari, D., Gaur, M., Yadav, A. B., García-Betancourt, M.-L., Abdel-Haleem, F. M., Bechelany, M. and Barhoum, A., *"Nanoparticle and Nanostructure Synthesis and Controlled Growth Methods," Nanomaterials*, 2022, 12(18), 3226.

[17] Gupta, D., Boora, A., Thakur, A. and Gupta, T. K., *"Green and sustainable synthesis of nanomaterials: recent advancements and limitations," Environ. Res.*, 2023, 231(3), 116316.

[18] El-Khawaga, A. M., Zidan, A. and Abd El-Mageed, A. I. A., *"Preparation methods of different nanomaterials for various potential applications: A review," J. Mol. Struct.*, 2023, 1281, 135148.

[19] Altammar, K. A., *"A review on nanoparticles: characteristics, synthesis, applications, and challenges," Front. Microbiol.*, 2023, 14, 1155622.

[20] Subramanian, Y., Abdalla, A. M., Azad, A. T., Omeiza, L. A., Dhanasekaran, A., Rahman, M. M., Eladl, A., Dawood, M. M. K. and Azad, A.-K., *"Challenges in the synthesis of ceramic nanoparticles and its applications in the energy sector,"* in *Advanced Ceramic Coatings for Energy Applications*, 1st ed., R. K. Gupta, A. Motallebzadeh, S. Kakooei, T. A. Nguyen and A. Behera, Eds., Elsevier, 2024, 117-152.

[DOI: 10.22068/ijmse.4451]

[21] Barooah, M., Kundu, S., Kumar, S., Katare, A., Borgohain, R., Uppaluri, R. V. S., Kundu, L. M. and Mandal, B., *"New generation mixed matrix membrane for CO_2 separation: Transition from binary to quaternary mixed matrix membrane," Chemosphere*, 2024, 354, 141653.

[22] Dyhr, K. and Willenbacher, N., *"Formulating Graphite-Filled PU Dispersions with Extended Shelf Life Using the Capillary Suspension Concept," Colloids and Interfaces*, 2025, 9(3), 26.

[23] Vijayan, A., Vishnu, J., Revathi, A., Shankar, B. and Sambhudevan, S., *"A review on hydroxyapatite fabrication: from powders to additive manufactured scaffolds," Biomater. Sci.*, 2025, 13(4), 913-945.

[24] Badr, M. H., Fadl, N. A., EL-Hamalawy, A. A. and Abouhaswa, A. S., *"Influence of annealing temperature on microstructure, magnetic and electrical properties of Ce doped cobalt ferrite nanoparticles," Ceram. Int.*, 2024, 50(12), 21367-21377.

[25] Zhang, R., Sun, L., Wang, Z., Hao, W., Cao, E. and Zhang, Y., *"Dielectric and magnetic properties of $CoFe_2O_4$ prepared by sol-gel auto-combustion method," Mater. Res. Bull.*, 2018, 98, 133-138.

[26] Silva, E. C., da Costa, J. C. M., Nascimento, M. C., Pereira, B. L., Passos, R. R. and Pocrifka, L. A., *"Influence of temperature on the preparation of $CoFe_2O_4$ by the sol-gel method and its application in electrochemical energy storage," J. Solid State Electrochem.*, 2020, 24(8), 1961-1968.

[27] Mishra, D., Nanda, J., Parida, S., Sankaran, K. J. and Ghadei, S., *"Effect of Y^{3+} and Co^{2+} co-doping on the structural, optical, magnetic and dielectric properties of $LaFeO_3$ nanoparticles," J. Sol-Gel Sci. Technol.*, 2024, 111(2), 381-394.

[28] Amiri, S. and Shokrollahi, H., *"Magnetic and structural properties of RE doped Co-ferrite (RE=Nd, Eu, and Gd) nano-particles synthesized by co-precipitation," J. Magn. Magn. Mater.*, 2013, 345, 18-23.

[29] Rezlescu, N., Rezlescu, E., Tudorache, F. and Popa, P. D., *"MgCu nanocrystalline ceramic with La^{3+} and Y^{3+} ionic substitutions used as humidity sensor," J. Optoelectron. Adv. Mater.*, 2004, 6(2), 695-698.

[30] Kumar, P., Pathak, S., Singh, A., Jain, K., Khanduri, H., Wang, L., Kim, S.-K. and Pant, R. P., *"Observation of intrinsic fluorescence in cobalt ferrite magnetic nanoparticles by Mn2+ substitution and tuning the spin dynamics by cation distribution," J. Mater. Chem. C*, 2022, 10(35), 12652-12679.

[31] Paswan, S. K., Kumari, S., Kar, M., Singh, A., Pathak, H., Borah, J. P. and Kumar, L., *"Optimization of structure-property relationships in nickel ferrite nanoparticles annealed at different temperature," J. Phys. Chem. Solids*, 2021, 151, 109928.

[32] Patta, G. R., Kumar, V. R., Ragavaiah, B. V. and Veeraiah, N., *"A critical study on the magnetic properties of ultrafine cobalt ferrite nanoparticles synthesized by polyethylene glycol assisted sol–gel method," Appl. Phys. A Mater. Sci. Process.*, 2020, 126(1), 64.

[33] Yadav, D., Gahlawat, R. and Shukla, R., *"A comprehensive analysis of the impact of annealing temperature variation on the structural, optical, morphological, magnetic, and photocatalytic properties of $CoFe_2O_4$ nanoparticles," Ionics*, 2024, 30(10), 6559-6574.

[34] Sakib, M. S., Rahman, M. N., Hossain, M. A. and Rahman, M. R., *"Effect of annealing on the structural, morphological, optical, magnetic, and dielectric properties of nickel-doped cobalt nanoferrites for electronic applications," Phys. Open*, 2025, 22, 100250.

[35] Sheikh, F. A., Asghar, H.M.N.-ul-H.K., Khalid, M., Gilani, Z. A., Ali, S. M., Khan, N.-ul-H., Shar, M. A., Mufti, H. and Alhazaa, A., *"Dielectrically modified Dy^{3+} substituted nickel-cobalt ferrites for high frequency devices," Phys. B Condens. Matter.*, 2023, 652, 414656.

[36] Ivanova, O. S., Edelman, I. S., Zharkov, S. M., Vorobyev, S. A., Andryushchenko, T. A., Molokeev, M. S., Sukhachev, A. L., Lin, C.-R., Chen, Y.-Z. and Huang, B-X., *"Impact of annealing temperature on the structure, magnetic properties, and organic dyes adsorption capacity of Fe0.5Co2.5O4 nanoparticles obtained by combustion," J. Alloys Compd.*, 2025, 1011, 178421.

[DOI: 10.22068/ijmse.4451]

[37] Prasad, G., Srinivas, Ch., Rani, P. V., Kumar, E. R., Singh, S., Meena, S. S. and Sastry, D. L., *"Green synthesis of CoFe2O4 nanoparticles assisted with bio-waste (Gomutram): Sintering effect on the properties of structural, microstructural and vibrational bands," J. Indian Chem. Soc.*, 2024, 101(5), 101151.

[38] Hameed, M. A. and Harbbi, K. H., *"Studying the Change in the Dislocation Density and the Burger Vector when the Temperature Changes Using the Method of Analysis X-Ray Diffraction Patterns," Ibn Al-Haitham J. Pure Appl. Sci.*, 2025, 38(1), 161-173.

[39] Routray, K. L., Saha, S. and Behera, D., *"Rare-earth (La3+) substitution induced changes in the structural, dielectric and magnetic properties of nano-CoFe2O4 for high-frequency and magneto-recording devices," Appl. Phys. A Mater. Sci. Process.*, 2019, 125(5), 1-15.

[40] Senthilkumar, V., Vickraman, P., Jayachandran, M. and Sanjeeviraja, C., *"Structural and electrical studies of nano structured Sn1−x SbxO2 (x= 0.0, 1, 2.5, 4.5 and 7 at%) prepared by co-precipitation method," J. Mater. Sci. Mater. Electron.*, 2010, 21, 343-348.

[41] Shyamaldas, Bououdina, M. and Manoharan, C., *"Dependence of structure/morphology on electrical/magnetic properties of hydrothermally synthesised cobalt ferrite nanoparticles," J. Magn. Magn. Mater.*, 2020, 493, 165703.

[42] Dhaka, S., Kumar, S., Poonia, K., Singh, V., Dhaka, K. and Mund, H. S., *"Effect of annealing temperature on structural and magnetic properties of nano-cobalt ferrite," J. Mater. Sci. Mater. Electron.*, 2021, 32(12), 16392-16399.

[43] Farid, M. T., Ahmad, I., Aman, S., Kanwal, M., Murtaz, G., Ali, I., Ahmad, I. and Ishfaq, M., *"SEM, FTIR and dielectric properties of cobalt substituted spinel ferrites," J. Ovonic Res.*, 2015, 11(1), 1-10.

[44] Yattinahalli, S. S., Kapatkar, S. B. and Mathad, S. N., *"Structural and mechanical properties of a nano ferrite," Adv. Sci. Focus*, 2014, 2(1), 42-46.

[45] Mondal, P., Akter, S., Roy, P., Elius, I. B., Khan, M. N. I. and Sikder, S. S., *"Tunable annealing effect to enhance structural and magnetic properties of spinel cobalt magnesium ferrite nanoparticles," AIP Adv.*, 2024, 14(10), 1-14.

[46] Kadam, R. H., Borade, R. B., Mane, M. L., Mane, D. R., Batoo, K. M. and Shirsath, S. E., *"Structural, mechanical, dielectric properties and magnetic interactions in Dy3+-substituted Co-Cu-Zn nanoferrites," RSC Adv.*, 2020, 10(47), 27911-27922.

[47] Hashim, M., Boda, N., Ahmed, A., Sharma, S. K., Ravinder, D., Sumalatha, E., Ul-Hamid, A., Ismail, M. M., Chaman, M., Shirsath, S. E., Kumar, R., Kumar, S., Meena, S. S. and Nasir, M., *"Influence of samarium doping on structural, elastic, magnetic, dielectric, and electrical properties of nanocrystalline cobalt ferrite," Appl. Phys. A Mater. Sci. Process.*, 2021, 127(7), 1-15.

[48] Singh, A. K., Goel, T. C., Mendiratta, R. G., Thakur, O. P. and Prakash, C., *"Dielectric properties of Mn-substituted Ni–Zn ferrites," J. Appl. Phys.*, 2002, 91(10), 6626-6629.

[49] Jabbar, R., Shahatha, S. H., Taieh, N. K., Magid, B. and Showard, A. F., *"Preparation and study of the effect of pH value on structural, morphological, electrical and magnetic properties of CoFe2O4 nanoparticles prepared by sol-gel precipitation method," Ceram. Int.*, 2024, 50, 31114-31123.

[50] Koops, C. G., *"On the dispersion of resistivity and dielectric constant of some semiconductors at audiofrequencies," Phys. Rev.*, 1951, 83(1), 121.

[51] Thomas, N., Jithin, P. V., Sudheesh, V. D. and Sebastian, V., *"Magnetic and dielectric properties of magnesium substituted cobalt ferrite samples synthesized via one step calcination free solution combustion method," Ceram. Int.*, 2017, 43(9), 7305-7310.

[52] Hench, L. L. and West, J. K., *Principles of Electronic Ceramics*, 1st ed., Wiley, New York, 1990, 576.

[DOI: 10.22068/ijmse.4451]

[53] Mohammad, A. M., Ali Ridha, S. M. and Mubarak, T. H., *"Dielectric Properties of Cr-Substituted Cobalt Ferrite Nanoparticles Synthesis by Citrate-Gel Auto Combustion Method," Int. J. Appl. Eng. Res.*, 2018, 13(8), 6026-6035.

[54] Pandey, B., Litterst, F. J. and Baggio-Saitovitch, E. M., *"Preferential spin canting in nanosize zinc ferrite," J. Magn. Magn. Mater.*, 2015, 385, 412-417.

[55] Muscas, G., Yaacoub, N., Concas, G., Sayed, F., Sayed Hassan, R., Greneche, J. M., Cannas, C., Musinu, A., Foglietti, V., Casciardi, S., Sangregoriohe, C. and Peddis, D., *"Evolution of the magnetic structure with chemical composition in spinel iron oxide nanoparticles," Nanoscale*, 2015, 7(32), 13576-13585.

[56] Mohammed, A. J. and Hamdan, S. A., *"Study the Effect of Calcined Temperature on Structural, Optical and Magnetic Properties for Cobalt Ferrite Nanostructure," Mustansiriyah J. Pure Appl. Sci.*, 2024, 2(3), 116-135.

[57] Shamkhi, A. F. and Jabbar, H., *"Effect of Cobalt Ion Concentration and Thermal Annealing Temperature on Structural and Magnetic Properties of CoFe2O4 Nanoparticles," Plasmonics*, 2025, 20(1), 421-430.

[58] Shirsath, S. E., Liu, X., Yasukawa, Y., Li, S. and Morisako, A., *"Switching of magnetic easy-axis using crystal orientation for large perpendicular coercivity in CoFe2O4 thin film," Sci. Rep.*, 2016, 6(1), 30074.

[59] Wohlfarth, E. P. and Buschow, K. H. J., *Ferromagnetic Materials: A Handbook on the Properties of Magnetically Ordered Substances*, 1st ed., E. P. Wohlfarth and K. H. J. Buschow, Eds., North-Holland Publishing Company, Amsterdam, Netherlands, 1991, 832.

[60] Islam, M., Khan, M. K. R., Kumar, A., Rahman, M. M., Abdullah-Al-Mamun, M., Rashid, R., Haque, M. M. and Sarker, M. S. I., *"Sol-Gel Route for the Synthesis of CoFe2-xErxO4 Nanocrystalline Ferrites and the Investigation of Structural and Magnetic Properties for Magnetic Device Applications," ACS Omega*, 2022, 7(24), 20731-20740.

[61] Chandra, G., Srivastava, R. C., Reddy, V. R. and Agrawal, H. M., *"Effect of sintering temperature on magnetization and Mössbauer parameters of cobalt ferrite nanoparticles," J. Magn. Magn. Mater.*, 2017, 427, 225-229.

[62] Kareem, S. J. and Rajeh, A. A. H., *"The Effect of Catalyst Type on The Microstructure and Magnetic Properties of Synthesized Hard Cobalt Ferrite Nanoparticles," Eng. Sci.*, 2018, 26, 282-291.

[63] Lin, J., Zhang, J., Sun, H., Lin, Q., Guo, Z., Yang, H. and He, Y., *"Structural and magnetic property of Cr3+ substituted cobalt ferrite nanomaterials prepared by the sol-gel method," Materials (Basel)*, 2018, 11(11). 2095.

[64] Venturini, J., Wermuth, T. B., Machado, M. C., Arcaro, S., Alves, A. K., da Cas Viegas, A. and Bergmann, C. P., *"The influence of solvent composition in the sol-gel synthesis of cobalt ferrite (CoFe2O4): A route to tuning its magnetic and mechanical properties," J. Eur. Ceram. Soc.*, 2019, 39(12), 3442-3449.

[65] Riyatun, Kusumaningsih, T., Supriyanto, A. and Purnama, B., *"Temperature annealing dependence of structural, magnetic, and antibacterial properties of silver substituted cobalt ferrite nanoparticles produced by coprecipitation route," Mater. Res. Express*, 2023, 10(5), 056101.

[DOI: 10.22068/ijmse.4451]